Improved artifact rejection for simultaneous EEG/fMRI at 7T using a high EEG channel density and a vector beamformer

M. J. Brookes[1], K. J. Mullinger[1], G. B. Geirsdottir[1], C. M. Stevenson[1], P. G. Morris[1], and R. W. Bowtell[1]

[1]Sir Peter Mansfield Magnetic Resonance Centre, School of Physics and Astronomy, University of Nottingham, Nottingham, Nottinghamshire, United Kingdom

Introduction: Simultaneous recording of fMRI and EEG is an attractive way of imaging brain function with high spatio-temporal resolution. However, such measurements are difficult due to the EEG artifacts caused by the MR scanner. A number of techniques for artifact removal [1,2] have been described, however even after correction residual artifacts remain in EEG data, particularly when measurements are made at high field. Previously we have shown [3] that the application of a vector beamformer to EEG data allows source localization of the electrical response, extraction of the timecourse of neuronal activity, and rejection of residual gradient and pulse artifacts. In this work, using both an EEG phantom and human recordings, we show that the signal to noise ratio of beamformer-reconstructed estimates of electrical activity is improved by the use of increased numbers of EEG channels. Furthermore, we show that the beamformer approach, applied to 64 channel concurrent EEG/fMRI recordings in a median nerve stimulation experiment, allows the robust measurement of low amplitude, high frequency gamma band effects.

Theory: Using a vector beamformer, a 3D estimate of source strength $\mathbf{Q}(\mathbf{r}, t)$ at location $\mathbf{r}$ and time t is made by a weighted sum of sensor measurements such that $\hat{\mathbf{Q}}(\mathbf{r},t) = \mathbf{W}(\mathbf{r})\mathbf{m}(t)$ where $\mathbf{W}(\mathbf{r})$ is a $3xM$ matrix of weighting parameters given by $\mathbf{W}(\mathbf{r})^T = \left[\mathbf{L}(\mathbf{r})^T \mathbf{C}^{-1}\mathbf{L}(\mathbf{r})\right]^{-1}\mathbf{L}(\mathbf{r})^T\mathbf{C}^{-1}$. M is the number of EEG channels and the $3xM$ matrix $\mathbf{L}(\mathbf{r})$ contains the EEG forward solutions for unit dipoles at location $\mathbf{r}$ with orthogonal orientations x, y, and z. The MxM matrix $\mathbf{C}$ represents the data covariance matrix. The beamformer reduces residual artifacts since any signal that does not originate from the location of interest, $\mathbf{r}$, will be rejected and not appear in $\hat{\mathbf{Q}}(\mathbf{r})$. In addition, as the number of channels available is increased, the correlation between the spatial topography of current dipole sources in the brain and the MR imaging artifacts is decreased. This means that the level of artifact rejection is increased.

Methods: ***EEG Phantom experiment:*** A 1cm long current dipole was placed within a spherical phantom (radius 10cm) and oriented in the x-y plane. The phantom was made from 4 % w/v agar and 2.5 % glycerol dissolved in a 154 mol/L NaCl solution. The conductivity was 2.7±0.3S/m. A 9.9Hz sinusoidal current was applied to the dipole giving a p-p dipolar source strength of 23(±2)nAm. EEG data were recorded using a *Brain Products* 64 channel system with a sampling frequency of 5kHz. Echo planar images were acquired simultaneously using a 7T Philips Achieva MR scanner (TR = 2.2s; TE = 25ms; 96x96 matrix; in plane resolution = 2mm; 20slices; slice width 2mm.) The scanner and EEG clocks were synchronised for improved artifact correction [4]. The EEG electrode locations on the phantom were found using a 3D digitiser (polhemus isotrack)

Initial correction of EEG data was performed in *Brain Vision Analyzer* and involved gradient correction using averaged artifact subtraction [2]. A vector beamformer was then applied. Lead field calculations were based on a single conducting sphere model [5]. A Ŧ stat beamformer image [3] was used to localize the dipole. Beamformer timecourse estimates were made with the location of interest selected at the peak in the Ŧ stat image. The number of channels used in the beamformer algorithm was varied between 15 and 63. For each channel count, 400 iterations of the algorithm were run using 400 randomly selected channels sets. On each iteration, an estimate of the beamformer SNR was derived from the height of the 9.9Hz peak divided by the integral of the power spectrum between 0 and 100Hz. For each channel count, the average SNR and associated error was compared to the single channel recording with the highest measured SNR.

Median Nerve experiment: Two subjects took part in the study. EEG data were recorded using the 64 channel EEG system. fMRI data were acquired simultaneously at 7T with imaging parameters as described above. The paradigm involved electrical stimulation of the right median nerve. A single trial comprised 8s of 2Hz electrical stimulation followed by 8s rest and the experiment comprised 30 trials. Initial correction of EEG data was performed using *Brain Vision Analyzer* and involved averaging and subtracting gradient and pulse artifacts [2]. The EEG beamformer algorithm was then applied using a triple sphere head model to account for the conductivity profile of the brain, skull and scalp [5]. Ŧ stat images were derived in order to show the location of the maximum 1-40Hz evoked response. EEG data were then frequency filtered between 1 and 40Hz (evoked response) and 30 – 50Hz (gamma band). For both frequency bands, beamformer estimated timecourses were extracted from regions of interest derived from the Ŧ stat map. In both cases two separate channel sets incorporating either 30 or 63 electrodes (following an equidistant montage) were used.

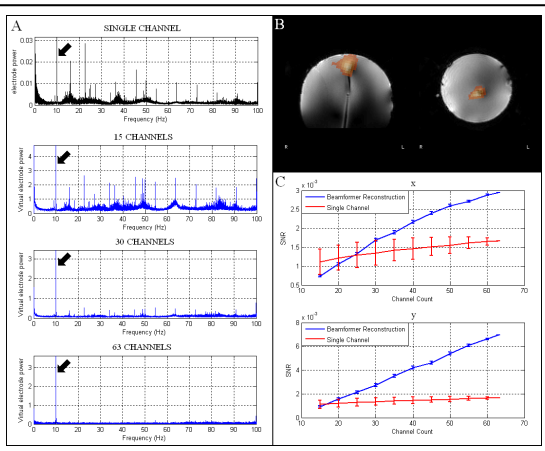

Figure 1. Results from the initial phantom experiments

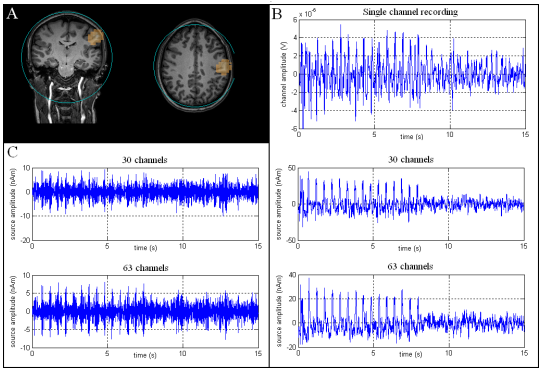

Figure 2. The results of the median nerve experiment

Results and discussion: Fig. 1B shows the source localisation of the dipole inside the phantom. The location of the maximum in the Ŧ stat map was found to coincide with the location of the dipole measured in the MR image. The upper panel of Fig. 1A shows a power spectrum taken from the single EEG channel exhibiting the highest SNR. The lower three panels show spectra from y-oriented beamformer estimates of source power made using 15, 30 and 63 channels. Fig. 1C shows SNR estimates as a function of the number of channels used. The SNR for the best available single channel (red) and the beamformer estimates (blue) are shown . The upper plot shows the SNR of the x-oriented beamformer estimate and the lower plot shows the y-oriented equivalent. As the dipole was oriented in the x-y plane, the z-oriented SNR is not shown. These results demonstrate that the SNR increases with channel count. Fig. 2 shows the results from the median nerve experiment. Fig. 2A shows the Ŧ stat image of the spatial location of the evoked response in Subject 1. Fig. 2B shows the timecourse of the trial averaged evoked response for the same subject. The upper plot shows the averaged evoked response at the channel level whilst the lower two plots show the x-oriented beamformer estimated average timecourse. Beamformer estimates were made using the location derived from the Ŧ stat images, using both 30 and 63 channels. Fig. 2C shows the z-oriented beamformer estimate of the gamma (30-50Hz) power, reconstructed using 30 and 63 channels for subject 2. Figs. 2B and 2C, clearly demonstrate the improvement in SNR with increasing channel count. Notice also that gamma band activity is not clear in the 30 channel data from Subject 2, but is clearly manifested when the channel count is increased to 64. This was not the case for subject 1 for whom the gamma response was observable using 30 or 63 channels.

Conclusion: We have shown, using an EEG phantom and human recordings, that the SNR of concurrent EEG/fMRI data is improved significantly by use of a beamformer and high EEG channel density. This approach allows for measurement of gamma band effects in a median nerve stimulation experiment conducted at 7T.

References: 1) Naizy RK. Et al. Neuroimage 2005;28(3):720-737. 2) Allen *et al*. Neuroimage **12**:230-239,2000. 3) Brookes et al. Proc. ISMRM, Berlin, 2007 Abs 699. 4) Mandelkow, H. et al. Neuroimage 32 (3) 1120-1126. 2006. 5) Zhang, Phys. Med. Biol. 40:335-349. 1995.